Int. J. Electrochem. Sci., 17 **(2022)** Article Number: 221140, doi: 10.20964/2022.11.40

International Journal of
ELECTROCHEMICAL
SCIENCE
www.electrochemsci.org

Short Communication

Electrodeposition of Ni-Co-Fe-P Alloy Coating on Q345 Steel Welded Joint and Its Corrosion Resistance in Acidic Chloride Solution

Lingguo Wang[1], *Yunfei Song*[2,*]

Hebei Chemical & Pharmaceutical College, Shijiazhuang 050026, China
[*]E-mail: Tech_wang0500@163.com

Received: 17 August 2022 / *Accepted:* 19 September 2022 / *Published:* 10 October 2022

To improve the corrosion resistance of Q345 steel welded joint in acidic chloride solution, Ni-Co-Fe-P alloy coating was prepared on the surface of welded joint by electrodeposition technology as a protection coating. Scanning electron microscope, energy dispersive spectrometer, transmission electron microscope and X-ray diffractometer were used to characterize and analyze the surface morphology, composition and structure of the Ni-Co-Fe-P alloy coating, and the corrosion resistance of Q345 steel substrate, Q345 steel welded joint and Ni-Co-Fe-P alloy coating was compared and evaluated in 3.5% sodium chloride + 2% hydrochloric acidic solution. The results show that the Ni-Co-Fe-P alloy coating to be relatively flat with a dense nanocrystalline structure that evenly covers the welded joint. In 3.5% sodium chloride + 2% hydrochloric acidic solution, the corrosion current density of Ni-Co-Fe-P alloy coating is only 1.16×10^{-6} A/cm^2, which is much lower than that of Q345 steel substrate and Q345 steel welded joint. The polarization resistance, charge transfer resistance and low-frequency impedance value of the Ni-Co-Fe-P alloy coating reaches 8.36×10^4 Ω·cm^2, 4.27×10^3 Ω·cm^2 and 5.51×10^3 Ω·cm^2, respectively, which are higher than those of Q345 steel substrate and Q345 steel welded joint. The Ni-Co-Fe-P alloy coating with nanocrystalline dense structure covers the Q345 steel substrate and welded joint completely, blocking the penetration and diffusion of corrosive ions as a means of effectively delaying the development of electrochemical corrosion process, resulting in excellent corrosion resistance.

Keywords: Ni-Co-Fe-P alloy coating; Electrodeposition; Q345 steel welded joint; Acidic chloride solution

1. INTRODUCTION

The welded components made from Q345 steel are widely used in vehicles, bridges, ships and chemical industries [1-3]. Welded joints are areas of weakness in such components. Due to the uneven heating during the welding process and the formation of iron-based intermetallic compounds or the

precipitation of ferrite, the corrosion resistance of welded joints is weakened significantly [4-8]. Following exposure to seawater, acid or alkaline solution, it is incredibly likely that the corrosion phenomenon of welded joints will occur and the degree of corrosion can be quite severe. Therefore, taking measures to improve the corrosion resistance of welded joints and help ensure the service life of welded components is of great practical significance.

In recent years, several studies have proven that surface treatment is an effective measure to improve the corrosion resistance of steel welded joints. For example, Gu et al. [9] used laser beam heating and powder injection technology to treat steel welded joint, effectively improving the corrosion resistance of the welded joint. Borko et al. [10] used the manganese phosphating technology to treat steel welded joint, a continuous and uniform manganese phosphating film with fine grains was prepared on the surface of welded joint, which significantly improved the corrosion resistance of welded joint in sodium sulfate solution. Das et al. [11] found that magnetic coating can play the role of a protective coating for steel welded joint after noting that it has a significant inhibitory effect on the corrosion of welded joint in marine environment. Hammi et al. [12] found that alumina composite coating that is prepared by coating technology can play a good protective effect on the surface of welded joint while preventing the penetration of corrosive medium and the formation of corrosion products through the formation of a protective coating. This slows down the corrosion of welded joint in dilute hydrochloric acid solution.

Electrodeposition is a surface treatment technology that has the advantages of simple operation and good controllability, enabling the realisation of the surface treatment of welded joints with complex structures, and also having broad application prospects [13-15]. The alloy coating has good corrosion resistance, particularly the corrosion resistance of the quaternary alloy mixed with nonmetal is very excellent. This paper focuses on electrodeposition of Ni-Co-Fe-P quaternary alloy coating on the surface of Q345 steel welded joint. The corrosion resistance of Q345 steel substrate, Q345 steel welded joint and the Ni-Co-Fe-P alloy coating in acidic chloride solution was tested and compared by electrochemical method with the aim of providing experimental data support to improve the corrosion resistance of steel welded joints.

2. EXPERIMENTAL MATERIALS AND METHODS

2.1 Materials

Table 1. Solution composition and process conditions for oil removal and pickling processes

Process	Solution composition	Process conditions
Oil removal	Na_2CO_3 15 g/L NaOH 8 g/L Na_3PO_4 22 g/L	60℃, 5 min
Pickling	hydrochloric acid (volume fraction 10%)	Room temperature, 1 min

The experimental sample consisted of two 15 mm×30 mm×3 mm rectangular Q345 steel plates that were welded together. The welded joint samples were prepared by cutting them parallel to the weld direction. The samples were successively processed by polishing, oil removal, pickling, water washing and drying. Table 1 shows the solution composition and process conditions used for oil removal and pickling processes.

2.2 Electrodeposition of Ni-Co-Fe-P alloy coating

The plating solution was prepared using analytical pure nickel sulfate, nickel chloride, ferrous sulfate, cobalt sulfate, boric acid, phosphoric acid, citric acid, thiourea and sodium dodecyl sulfate. The main composition is shown in Table 2. Before the experiment, the anode was also cleaned, washed and dried successively. The anode and cathode were placed perpendicular to each other with a distance of 3 cm. The surface area of the anode was about two times larger than that of the cathode. During electrodeposition of Ni-Co-Fe-P alloy coating, the anode is connected to the positive pole of the power supply, and the cathode is connected to the negative pole of the power supply. The constant current mode was set and the plating solution was continuously stirred by magnetic stirrer. The electrodeposition process conditions are as follows: current density 2 A/dm^2, plating solution temperature 65℃, stirring rate 400 r/min, electrodeposition time 1.5 h. After electrodeposition, the Q345 steel welded joint samples were cleaned, dried and tested.

Table 2. Main composition of plating solution

Chemical agents	Concentration/ ($g \cdot L^{-1}$)
nickel sulfate	125
nickel chloride	30
ferrous sulfate	20
cobalt sulfate	15
boric acid	35
phosphoric acid	30
citric acid	10
thiourea	0.02
sodium dodecyl sulfate	0.06

2.3 Performance testing

2.3.1 Surface morphology and composition of Q345 steel welded joint and Ni-Co-Fe-P alloy coating

Quanta FEG450 scanning electron microscope was used to characterize the surface morphology of Q345 steel substrate, Q345 steel welded joint and the Ni-Co-Fe-P alloy coating. The acceleration voltage was 10 kV and the magnification was 5000 times. XFlash 5030 energy dispersive spectrometer was set the surface scanning mode to analyze the composition of Ni-Co-Fe-P alloy coating under the condition of 40 kV with surface scanning mode.

2.3.2 Structure of Ni-Co-Fe-P alloy coating

The structure of Ni-Co-Fe-P alloy coating was characterized by D8 Advance X-ray diffractometer combined with Tecnai G2 20S-Twin transmission electron microscope. The voltage and current of X-ray diffractometer were set to 40 kV and 40 mA, scanning from 20° to 100° with the scan rate of 4 °/min.

The XRD spectrum test data were imported into Jade software to analyze the crystal plane and crystal structure of Ni-Co-Fe-P alloy coating. The images captured by transmission electron microscopy were processed by Nano Measurer software, and then the grain size distribution of Ni-Co-Fe-P alloy coating was calculated.

2.3.3 Corrosion resistance of Q345 steel welded joint and Ni-Co-Fe-P alloy coating in acidic chloride solution

The polarization curves and electrochemical impedance spectroscopy of Q345 steel substrate, Q345 steel welded joint and Ni-Co-Fe-P alloy coating in 3.5% sodium chloride + 2% hydrochloric acidic solution were tested by electrochemical method. Before electrochemical test, the surface of the samples were lightly polished and cleaned to eliminate the influence of surface condition on the test results. The epoxy resin was used to seal each sample. The exposed working face size of Q345 steel substrate, Q345 steel welded joint and Ni-Co-Fe-P alloy coating is 1 cm×1 cm. The reference electrode was saturated with calomel electrode and the auxiliary electrode was platinum electrode. The scanning rate of polarization curve was 1 mV/s, and the scanning range was ±250 mV relative to the open circuit potential. Electrochemical impedance spectroscopy was tested under the condition of 10 mV amplitude and the frequency range of 10^{5}~10^{-2} Hz.

Polarization curves test data were imported into PowerSuite software for preprocessing and analysis, and electrochemical impedance spectroscopy test data were imported into ZSimpWin software for preprocessing and analysis.

According to the polarization curves analysis results (including corrosion potential, corrosion current density and polarization resistance) and electrochemical impedance spectroscopy analysis results (including charge transfer resistance and low-frequency impedance value), the corrosion resistance of Q345 steel substrate, Q345 steel welded joint and Ni-Co-Fe-P alloy coating in acidic chloride solution was compared.

3. RESULTS AND DISCUSSION

3.1 Surface morphology and composition of Q345 steel welded joint and Ni-Co-Fe-P alloy coating

Figure 1 shows the appearance and surface morphology of Q345 steel substrate, Q345 steel welded joint and Ni-Co-Fe-P alloy coating. Comparing Figure 1(a), 1(b) and 1(c), it can be seen that the Ni-Co-Fe-P alloy coating is more uniform and smooth, and it has good coverage on both the Q345

steel substrate and welded joint. Figure 1(c) shows that there are no obvious defects including pinholes or cracks on the surface of Ni-Co-Fe-P alloy coating, and the grains are cell-like and tightly combined, exhibiting good compactness. The similar surface morphology of Co-Ni alloy coating, Ni-Fe alloy coating and Co-Ni-Fe alloy coating has been reported in some previous literatures [16-20].

Figure 1. Appearance and surface morphology of Q345 steel substrate, Q345 steel welded joint and Ni-Co-Fe-P alloy coating

Figure 2 shows the EDS spectrum of Ni-Co-Fe-P alloy coating. It can be seen from Figure 2 that the EDS spectrum shows characteristic peaks of Ni, Co, Fe, P, C and O elements. Among them, C and O elements were introduced due to the phenomenon of adsorption on the surface of the sample during storage. After deducting these two elements, it is known that the composition of Ni-Co-Fe-P alloy coating is mainly Ni, Co, Fe and P elements. The mass fraction of Ni element is the highest, reaching 82.7%, while the mass fraction of Co and Fe elements are relatively low, about 6% and 4%, respectively. Previous studies have found that the mass fraction of P element affects the crystal structure of nickel-based alloy coatings [21-23]. When the mass fraction of P element is below 8%, the nickel-based alloy coatings generally have a crystalline structure.

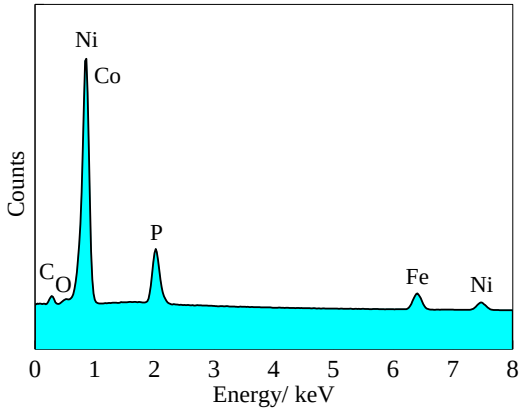

Figure 2. EDS spectrum of Ni-Co-Fe-P alloy coating

3.2 Structure of Ni-Co-Fe-P alloy coating

Figure 3 shows the XRD spectrum of Ni-Co-Fe-P alloy coating. It can be seen from Figure 3 that the XRD spectrum shows four diffraction peaks, corresponding to the (111), (200), (311), (222) crystal planes, with diffraction angle of approximately 45°, 52°, 93°, and 98°, respectively. This demonstrates that the Ni-Co-Fe-P alloy coating has a crystalline structure. Among them, the (111) and (200) diffraction peaks have obvious peak shape broadening, thereby confirming the fine grains of the Ni-Co-Fe-P alloy coating. Electrodeposition of Ni-Co-Fe-P alloy coating is abnormal co-deposition and Co, Fe and P may enter into Ni lattice to form substitutional solid solution, leading to a dense structure in Ni-Co-Fe-P alloy coating [24-26]. Figure 4 shows the TEM bright field image, selected area diffraction pattern and grain size distribution of Ni-Co-Fe-P alloy coating. It can be seen from Figure 4(b) that the selected area diffraction pattern presents a nested continuous ring, further confirming the fineness and compactness of the grains of Ni-Co-Fe-P alloy coating. It can be seen from Figure 4(c) that approximately 77.5% of the grain size is in the numerical range of 40~70 nm, and only approximately 2.8% of the grain size is close to 80 nm.

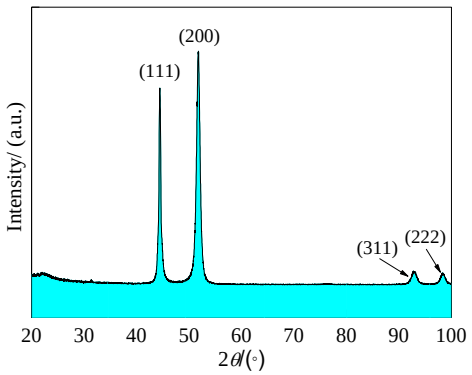

Figure 3. XRD spectrum of Ni-Co-Fe-P alloy coating

From the grain size distribution statistics, the average grain size can be calculated as 51.6 nm. In conclusion, Ni-Co-Fe-P alloy coating has fine grains with nanocrystalline dense structure. Nanocrystalline or crystalline structure of Ni-Co-Fe alloy coatings are prepared and reported in some previous literatures [27-28]. For example, Chen fabricated a nanocrystalline $Co_{45}Ni_{10}Fe_{24}$ alloy coating using cyclic voltammetry technique from the solutions containing sulfate [29].

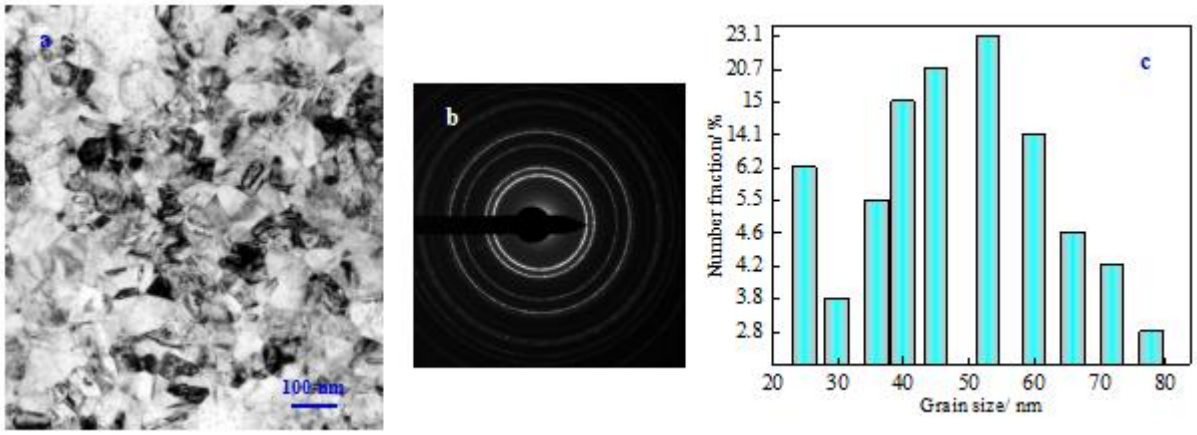

Figure 4. TEM bright field image, selected diffraction pattern and grain size distribution of Ni-Co-Fe-P alloy coating: a-TEM bright field image; b-Selected diffraction pattern; c-grain size distribution

3.3 Corrosion resistance of Q345 steel welded joint and Ni-Co-Fe-P alloy coating in acidic chloride solution

3.3.1 Polarization curve analysis

Figure 5 shows the polarization curves of Q345 steel substrate, Q345 steel welded joint and Ni-Co-Fe-P alloy coating in 3.5% sodium chloride +2% hydrochloric acidic solution. As can be seen from Figure 5, Q345 steel substrate, Q345 steel welded joint and Ni-Co-Fe-P alloy coating all show the characteristics of active dissolution. Compared with Q345 steel substrate, the corrosion potential of Q345 steel welded joint shifts negatively, indicating that the welded joint has a strong tendency to corrosion. The reason is that residual stress and crevice are easy to be generated by uneven heating during welding, which leads to stress corrosion and crevice corrosion leading to the fast development of corrosion. Some researchers also investigated the corrosion resistance of steel welded joint [30-32].

Table 3 lists the electrochemical parameters related to the polarization curve, and the polarization resistance is calculated according to the Stern-Geary formula. It can be seen from Table 3 that the corrosion potential of Ni-Co-Fe-P alloy coating has a positive shift of 84 mV and 125 mV compared with that of Q345 steel substrate and Q345 steel welded joint, respectively. The corrosion current of Ni-Co-Fe-P alloy coating is only 1.16×10^{-6} A/cm^2, which is more than an order of magnitude lower than that of Q345 steel substrate and Q345 steel welded joint. The positive shift of corrosion potential and the obvious decrease of corrosion current density indicate that the Ni-Co-Fe-P alloy coating on the surface of Q345 steel substrate and welded joint can effectively reduce the

corrosion tendency. The Ni-Co-Fe-P alloy coating completely covers Q345 steel substrate and welded joint which can shield and block corrosive ions to limit the penetration and diffusion of corrosive ions in contact with Q345 steel substrate and welded joint, thereby increasing corrosion resistance.

It can also be seen from Table 3 that the polarization resistance of Ni-Co-Fe-P alloy coating reaches 8.36×10^4 $\Omega\cdot cm^2$, which is about five times and seven times higher than that of Q345 steel substrate and Q345 steel welded joint, respectively. The higher polarization resistance indicates that the electrochemical reaction of Ni-Co-Fe-P alloy coating is greatly hindered, and the corrosion process develops slowly, which further confirms that Ni-Co-Fe-P alloy coating can provide good corrosion protection for Q345 steel welded joint.

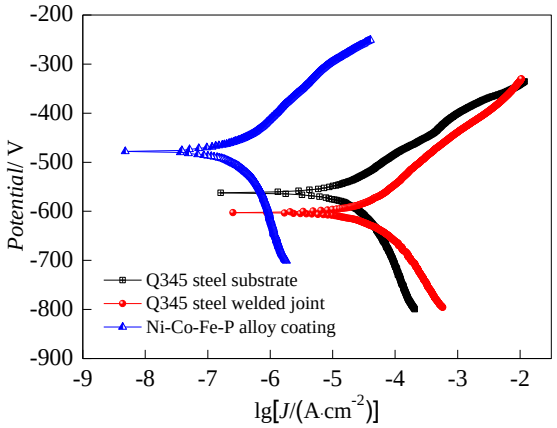

Figure 5. Polarization curves of Q345 steel substrate, Q345 steel welded joint and Ni-Co-Fe-P alloy coating in 3.5% sodium chloride +2% hydrochloric acidic solution

Table 3. Electrochemical parameters related to polarization curve

Different samples	Corrosion potential / V	Corrosion current density / ($A\cdot cm^{-2}$)	Polarization resistance / ($\Omega\cdot cm^2$)
Q345 steel substrate	-0.562	3.60×10^{-5}	1.31×10^4
Q345 steel welded joint	-0.603	5.86×10^{-5}	1.04×10^4
Ni-Co-Fe-P alloy coating	-0.478	1.16×10^{-6}	8.36×10^4

3.3.2 Electrochemical impedance spectroscopy analysis

Figure 6 shows the electrochemical impedance spectroscopy of Q345 steel substrate, Q345 steel welded joint and Ni-Co-Fe-P alloy coating in 3.5% sodium chloride +2% hydrochloric acidic solution. It can be seen from Figure 6(a) that the Nyquist diagram of Q345 steel substrate, Q345 steel welded joint and Ni-Co-Fe-P alloy coating all have almost semicircle resistance arcs. The different radius of capacitive reactance arc reflects the resistance of charge transfer during electrochemical corrosion. As can be seen from Figure 6(b), the low-frequency impedance value of Q345 steel substrate, Q345 steel welded joint and Ni-Co-Fe-P alloy coating gradually decrease with the increase

of frequency and then maintain a basically constant trend. Generally, the impedance value at low frequency (10^{-2} Hz) reflects the ability of the materials to shield against corrosive media [33-35].

Combined with Figure 6 and Table 4, it can be seen that the Nyquist diagram of Ni-Co-Fe-P alloy coating presents the largest capacitive arc. The charge transfer resistance and low-frequency impedance value of Ni-Co-Fe-P alloy coating are significantly higher than those of the Q345 steel substrate and Q345 steel welded joint, respectively. This proves that the Ni-Co-Fe-P alloy coating has strong shielding and blocking ability against corrosive ions. Higher charge transfer resistance inhibits and slows down the electrochemical corrosion process. The relationship between higher charge transfer resistance and corrosion is studied in some literatures [36-38].

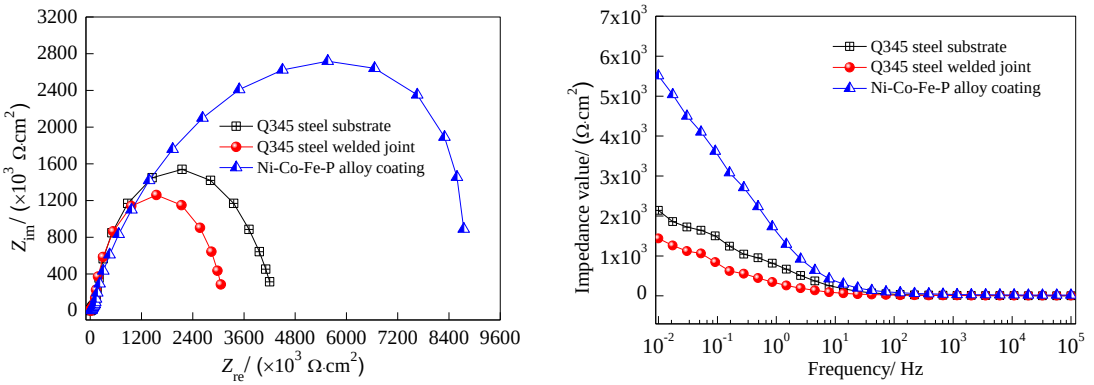

(a) Nyquist diagram (b) Frequency-impedance value diagram

Figure 6. Electrochemical impedance spectroscopy of Q345 steel substrate, Q345 steel welded joint and Ni-Co-Fe-P alloy coating in 3.5% sodium chloride +2% hydrochloric acidic solution

Table 4. Electrochemical parameters related to electrochemical impedance spectroscopy

Different samples	Charge transfer resistance/ (Ω·cm^2)	Low-frequency impedance value/ (Ω·cm^2)
Q345 steel substrate	2.05×10^3	2.14×10^3
Q345 steel welded joint	1.49×10^3	1.52×10^3
Ni-Co-Fe-P alloy coating	4.27×10^3	5.51×10^3

4. CONCLUSIONS

(1) Ni-Co-Fe-P alloy coating prepared by electrodeposition technology on the surface of Q345 steel welded joint is uniform and flat, with the composition of Ni, Co, Fe and P elements. The grains of Ni-Co-Fe-P alloy coating are similar to cell shape and tightly bonded with an average grain size of 51.6 nm. In 3.5% sodium chloride +2% hydrochloric acidic solution, the corrosion current density of Ni-Co-Fe-P alloy coating is only 1.16×10^{-6} A/cm^2, and the polarization resistance, charge transfer resistance and low-frequency impedance value are 8.36×10^4 Ω·cm^2, 4.27×10^3 Ω·cm^2 and 5.51×10^3 Ω·cm^2, respectively, which can effectively prevent the penetration diffusion of corrosive ions from

contacting with the Q345 steel substrate and Q345 steel welded joint to delay the development of electrochemical corrosion process.

(2) Compared with Q345 steel substrate and Q345 steel welded joint, the corrosion current density of Ni-Co-Fe-P alloy coating is reduced by more than one order of magnitude. The polarization resistance, charge transfer resistance and low-frequency impedance value of Ni-Co-Fe-P alloy coating are the highest indicating excellent corrosion resistance. Moreover, Ni-Co-Fe-P alloy coating has nanocrystalline dense structure and good coverage to the welded joint, offering excellent corrosion protection and significantly improving the corrosion resistance of Q345 steel welded joint in acidic chloride solution.

References

1. W. Chen, J. H. Ye, L. Jin, J. Jiang, K. Liu, M. Zhang, W. W. Chen and H. Zhang, *J. Constr. Steel Res.*, 175 (2020) 106366.
2. Z. W. Zhao, H. W. Zhang, L. Xian and H. Q. Liu, *Thin Walled Struct.*, 148 (2020) 106579.
3. B. A. Wang, N. Wang, Y. J. Yang, H. Zhong, M. Z. Ma, X. Y. Zhang and R. P. Liu, *Trans. Nonferrous Met. Soc. China*, 28 (2018) 1132.
4. F. Y. Gao, Z. J. Sun, S. L. Yang, P. Jiang and Z. Q. Liao, *Mater. Charact.*, 192 (2022) 112126.
5. M. N. Ilman, A. Widodo and N. A. Triwibowo, *J. Adv. Joining Processes*, 6 (2022) 100129.
6. Z. D. Wan, W. Dai, W. Guo, Q. Jia, H. Q. Zhang, J. L. Xue, L. C. Lin and P. Peng, *J. Manuf. Processes*, 80 (2022) 718.
7. K. L. Shen, W. C. Jiang, C. Sun, W. M. Zhao and J. B. Sun, *Corros. Sci.*, 206 (2022) 110532.
8. Q. Wang, X. B. Zhou, Q. Ma, T. Q. Wu, M. Liu, M. H. Zhang, Z. Li and F. C. Yin, *Corros. Sci.*, 202 (2022) 110313.
9. H. P. Gu and A. V. Gelder, *J. Laser Appl.*, 28 (2016) 022411.
10. K. Borko, F. Pastorek, M. N. Jachova and B. Hadzima, *Mater. Today:. Proc.*, 5 (2018) 26482.
11. C. R. Das and P. K. Jena, *Corros. Sci.*, 2 (1983) 1135.
12. M. Hammi, Y. Ziat, Z. Zarhri, C. Laghlimi and A. Moutcine, *Sci. Rep.*, 11 (2021) 12928.
13. S. T. Auwal, S. Ramesh, Z. Q. Zhang, J. Liu, C. W. Tan, S. M. Manladan, F. Yusof and F. Tarlochan, *J. Manuf. Processes*, 37 (2019) 251.
14. M. Hakamada, N. Miyazawa, Y. Kohashi, Y. Yamano and M. Mabuchi, *Procedia Manuf.,* 15 (2018) 1416.
15. M. F. D. Carvalho, E. P. Barbano and I. A. Carlos, *Surf. Coat. Technol.*, 262 (2015) 111.
16. Y. D. Yu, G. Y. Wei, H. L. Ge, L. Jiang, L. X. Sun, *Surf. Eng.*, 33 (2017) 483.
17. S. Thanikaikarasan, T. Mahalingam, T. Ahamad and S. M. Alshehri, *J. Saudi Chem. Soc.*, 24 (2020) 955.
18. J. Gong, S. Riemer, M. Kautzky and I. Tabakovic, *J. Magn. Magn. Mater.*, 398 (2016) 64.
19. B. Koo and B. Yoo, *Surf. Coat. Technol.*, 205 (2010) 740.
20. J. M. Li, Z. Zhang, J. F. Li, M. Z. Xue and Y. G. Liu, *Trans. Nonferrous Met. Soc. China*, 23 (2013) 674.
21. C. B. Wang, D. L. Wang, W. X. Chen and Y. Y. Wang, *Wear,* 253 (2002) 563.
22. P. Cojocaru, L. Magagnin, E. Gomez and E. Valles, *J. Alloys Compd.,* 503 (2010) 454.
23. L. Shen, M. Y. Xu, W. Jiang, M. B. Qiu, M. Z. Fan, G. B. Ji and Z. J. Tian, *Appl. Surf. Sci.,* 489 (2019) 25.
24. Y. C. Wu, K. Xu, Z. Y. Zhang, X. R. Dai, D. Y. Zhao, H. Zhu and A. B. Wang, *J. Electroanal. Chem.*, 905 (2022) 115967.
25. Y. D. Yu, G. Y. Wei, J. W. Lou, L. X. Sun, L. Jiang and H. L. Ge, *Surf. Eng.*, 28 (2021) 244.

26. J. Zhou, X. H. Meng, O. Y. Ping, R. Zhang, H. Y. Liu, C. M. Xu and Z. C. Liu, *J. Electroanal. Chem.*, 919 (2022) 116516.
27. W. Y. Huo, S. Q. Wang, F. Fang, S. Y. Tan, L. Kurpaska, Z. H. Xie, H. S. Kim and J. Q. Jiang, *J. Mater. Res. Technol.*, 20 (2022) 1677.
28. N. R. N. Masdek, Z. Salleh, Y. M. Taib, M. C. Murad and Z. Zulfarizan, *Mater. Today:. Proc.*, 16 (2019) 1919.
29. Y. Chen, Q. P. Wang, C. Cai, Y. N. Yuan, F. H. Cao, Z. Zhang and J. Q. Zhang, *Thin Solid Films*, 520 (2012) 3553.
30. S. L. Ding, M. C. Zhou, X. B. Liu, C. H. Liu and X. F. Zhang, *Mater. Sci. Eng., A*, 849 (2022) 143506.
31. D. Bai, F. D. Liu, H. Zhang and J. Liu, *Mater. Lett.*, 317 (2022) 132101.
32. Y. T. Ma, H. G. Dong, P. Li, J. Yang, B. S. Wu, X. H. Hao, Y. Q. Xia and G. B. Qi, *Corros. Sci.*, 194 (2022) 109936.
33. V. I. Kichigin, M. V. Polyakova, T. A. Syur, N. V. Bezmaternukh, O. P. Koshcheev and A. I. Rabinovich, *Prot. Met.*, 38 (2002) 563.
34. P. Slepski, M. Szocinski, G. Lentka and K. Darawicki, *Measurement*, 173 (2021) 108667.
35. P. Mishra, D. Yavas, A. F. Bastawros and K. R. Hebert, *Electrochim. Acta*, 346 (2020) 136232.
36. M. Moradi, G. Ghiara, R. Spotorno, D. Xu and P. Cristiani, *Electrochim. Acta*, 426 (2022) 140803.
37. E. Hamed, *Mater. Chem. Phys.*, 121 (2010) 70.
38. M. Kissi, M. Bouklah, B. Hammouti and M. Benkaddour, *Appl. Surf. Sci.*, 252 (2006) 4190.